Published in final edited form as:
Biotechnol Bioeng. 2012 October ; 109(10): 2651–2662. doi:10.1002/bit.24538.

pH, Redox Potential and Local Biofilm Potential Microenvironments Within *Geobacter sulfurreducens* Biofilms and Their Roles in Electron Transfer

Jerome T. Babauta, **Hung Duc Nguyen**, **Timothy D. Harrington**, **Ryan Renslow**, and **Haluk Beyenal**
The Gene and Linda Voiland School of Chemical Engineering and Bioengineering, Washington State University, PO Box 642710, Pullman, Washington 99164-2710

Abstract

The limitation of pH inside electrode-respiring biofilms is a well-known concept. However, little is known about how pH and redox potential are affected by increasing current inside biofilms respiring on electrodes. Quantifying the variations in pH and redox potential with increasing current is needed to determine how electron transfer is tied to proton transfer within the biofilm. In this research, we quantified pH and redox potential variations in electrode-respiring *Geobacter sulfurreducens* biofilms as a function of respiration rates, measured as current. We also characterized pH and redox potential at the counter electrode. We concluded that (1) pH continued to decrease in the biofilm through different growth phases, showing that the pH is not always a limiting factor in a biofilm and (2) decreasing pH and increasing redox potential at the biofilm electrode were associated only with the biofilm, demonstrating that *G. sulfurreducens* biofilms respire in a unique internal environment. Redox potential inside the biofilm was also compared to the local biofilm potential measured by a graphite microelectrode, where the tip of the micro-electrode was allowed to acclimatize inside the biofilm.

Keywords

Geobacter; biofilm; redox; hydrogen; electron transfer; bioelectrochemical system; microbial electrolysis cell (MEC)

Introduction

Electron transfer processes in biofilms respiring on electrodes play a critical role in microbial fuel cells (MFCs) and microbial electrolysis cells (MECs) (Liu et al., 2005; Logan et al., 2006; Rozendal et al., 2006). The goal of MFC studies is to increase power generation, while the goal of MEC studies is to increase hydrogen production. A fundamental knowledge of how cells in MFC/MEC biofilms transfer electrons to solid electrode surfaces could lead to the development of better-performing MFCs and MECs. *Shewanella oneidensis* MR-1 and *Geobacter sulfurreducens* are two model organisms capable of respiring on electrodes and are widely used in MFCs. It is believed that *G. sulfurreducens* transfers electrons directly, while *S. oneidensis* MR-1 transfers electrons using both mediated and direct mechanisms (Bond et al., 2002; Bond and Lovley, 2003;

Correspondence to: H. Beyenal telephone: 509-334-0896; fax: 509-335-4806; beyenal@wsu.edu.

Additional supporting information may be found in the online version of this article.

Bouhenni et al., 2010; Coursolle et al., 2010; Gorby et al., 2006; Marsili et al., 2008; Reguera et al., 2006; von Canstein et al., 2008). Regardless of whether electron transfer is direct or mediated, it is usually coupled with proton transfer to maintain electroneutrality in solution, which is expected to cause pH shifts in biofilms (Torres et al., 2008ab). In addition, if redox mediators (soluble or bound) transfer electrons, it is expected that the redox potential will increase towards the bottom of the biofilm (Babauta et al., 2011). For a biofilm respiring on an electrode while oxidizing an electron donor, both the pH and the redox potential are expected to change (Babauta et al., 2011). The relationship between pH and redox potential can be evaluated using the following equations:

$$[\mathrm{Ox}] + n\mathrm{e}^- + m[\mathrm{H}^+] \leftrightarrow [\mathrm{H}_m\mathrm{Red}] \quad (1)$$

$$E_\mathrm{h} = E^0 - \frac{59.16}{n} \log \frac{[H_m\mathrm{Red}]}{[\mathrm{Ox}]} - 59.16\frac{m}{n}\mathrm{pH} \quad (2)$$

where E_h is the redox potential (mV), E^0 is the standard redox potential (mV), [Ox] is the concentration of the oxidized species (M), $[H_m\mathrm{Red}]$ is the concentration of the reduced species (M), n is the number of electrons transferred, and m is the number of protons transferred. According to Equation (2), redox potential increases as pH decreases towards the bottom of an electrode-respiring biofilm. However, only redox couples involving protons can affect pH. Thus, pH may not be a good indicator of redox potential in complex systems such as electron transfer in biofilms. Therefore, it is critical to quantify pH and redox potential in the same biofilm to understand their role in electron transfer and proton transfer.

The literature is generally limited to bulk measurements of pH during current generation (Patil et al., 2010; Torres et al., 2008b). Torres et al. (2008b) observed increasing current densities with increasing pH and increasing buffer concentration. Patil et al. (2010) further showed that current generation was inhibited completely below a pH of 5 and above a pH of 11 (the maximum current was seen at pH 9). Variations in pH inside electrode-respiring *G. sulfurreducens* biofilms were measured by Franks et al. (2009): they observed the pH drop to 6.2 near the biofilm surface from 6.8 in the bulk. Picioreanu et al. (2010) developed a mathematical model to predict pH and redox potential in electrode-respiring biofilms grown in batch mode. For a current density of 0.2 A/m^2, a 200-mV increase in redox potential from the top of the biofilm to the bottom and a 0.03 pH change from the bulk to the bottom of the biofilm were predicted, but the model was not experimentally verified. Interestingly, their model indicated that for high proton mass transfer rates, current generation is limited by the biofilm at a carbonate buffer strength greater than 2 mM. Measuring pH and redox potentials in the same electrode-respiring biofilm could verify their model of proton transfer.

Microelectrodes offer an alternate, minimally invasive method of quantifying critical parameters inside biofilms. Recently, we used microelectrodes to quantify pH and redox potential profiles in electrode-respiring *S. oneidensis* MR-1 biofilms (Babauta et al., 2011). We found that there was no observable pH variation in the biofilm, while redox potential decreased towards the bottom of the biofilm, demonstrating the reducing capability of the biofilm. *G. sulfurreducens* biofilms generate higher current compared to *S. oneidensis* MR-1 biofilms, which should cause observable pH variations inside the biofilm. However, there is currently no information about redox potential variations in *G. sulfurreducens* biofilms respiring on electrodes.

The goal of this research was to (1) quantify pH and redox potential variations in electrode-respiring *G. sulfurreducens* biofilms through two growth stages and (2) quantify pH and redox potential variations at the counter electrode. The comprehensive information we

obtained in this way was different from using a mature biofilm and exposing it to varying experimental conditions. This allowed us to discover that pH was not always limiting biofilm growth as speculated in the literature. We grew *G. sulfurreducens* on a glassy carbon electrode located in a three-electrode bioreactor. The pH and redox potential profiles in the *G. sulfurreducens* biofilms were measured using recently developed microelectrodes (Babauta et al., 2011). Since the redox potential is a measure of the equilibrium potential of the soluble redox-active compounds in the biofilm, we also wanted to determine what the local potential inside the biofilm was when the biofilm equilibrated with the microelectrode tip (Fig. 1). Therefore, we used a graphite microelectrode to measure the local biofilm potential (LBP; Fig. 1). This microelectrode was made of a graphite tip at the end of a glass-covered carbon fiber and was left in the biofilm until the potential at the tip of the microelectrode reached equilibrium. We also polarized this microelectrode to connect it electronically to the biofilm matrix and measured the current and open circuit potentials (OCP). An illustration of microelectrodes measuring redox potential and LBP is shown in Figure 1. Redox potential was determined in a few seconds and was used to qualitatively measure the ratio between the oxidized and the reduced mediators. LBP was determined after the microelectrode tip had equilibrated with the biofilm, likely by depositing redox-active proteins or establishing electronic connections to the microelectrode tip (Malvankar et al., 2011; Strycharz-Glaven et al., 2011).

Materials and Methods

Bioelectrochemical Reactor

Biofilms were grown in a continuously fed, three-electrode bioreactor with recycle as shown in Figure 2. The working, counter, and reference electrodes were all in the same solution. The working electrode, on which *G. sulfurreducens* respired, was glassy carbon (SPI-Glas™ grade 11; 25 mm × 25 mm × 2 mm). The counter electrode was graphite (ground finish isomolded graphite plates, Glassmate grade GM-10, 25 mm × 25 mm × 3 mm, Poco Graphite, Inc., Decatur, TX), and the reference electrode was a Ag/AgCl wire that was observed to maintain a constant potential during the experiment, which measured +150 mV versus a saturated KCl Ag/AgCl reference. The use of a Ag/AgCl wire prevented the leak of KCl into the reactor and prevented possible contamination. All potentials reported in this study were adjusted to the saturated KCl Ag/AgCl reference. The reactor body was made of polycarbonate and autoclavable plastic connectors. Tygon tubing (Cole-Parmer, Vernon Hills, IL, catalog EW-06475-14, EW-06475-16) was used for the feed, waste, and recycle streams. Flow breakers were used in the feed and waste streams to prevent back contamination. A 0.2-μm filter was used at the gas inlet to sparge a mixture of N_2/CO_2 (80%/20%). Another 0.2-μm filter was used at the gas outlet to relieve pressure buildup. The polycarbonate lid was sealed with a thin layer of silicone rubber sealant 24 h prior to autoclaving for 20 min at 121°C. The growth medium was autoclaved separately in a 10-L carboy (Thermo Scientific, Waltham, MA, 2250-0020) for 100 min at 121°C. Once the biofilm reactor and growth medium cooled to room temperature, the 10-L carboy was aseptically connected to the biofilm reactor feed stream. The completed reactor system was placed in an incubator set to 30°C. The biofilm reactor was then inoculated. The dilution rate of the biofilm reactor was 6.1 hr^{-1}.

Inoculum and Growth Medium

G. sulfurreducens strain PCA (ATCC 51573) inoculum was grown under anaerobic conditions using the Hungate technique (Miller and Wolin, 1974) in a serum vial without shaking in the following growth medium: potassium chloride, 0.38 g/L; ammonium chloride, 0.2 g/L; sodium phosphate monobasic, 0.069 g/L; calcium chloride, 0.04 g/L; magnesium sulfate heptahydrate, 0.2 g/L; sodium carbonate, 2 g/L; Wolfe's vitamin

solution, 10 mL/L; modified Wolfe's mineral solution, 10 mL/L. Acetate (20 mM) was provided as the electron donor, and 40 mM fumarate (inoculum only) was the electron acceptor. When a visible layer of cells was observed at the bottom of the vial, the cells were ready for inoculation. The cultures were washed once with fumarate-free medium prior to inoculation. The same growth medium used in the inoculum was used to grow the biofilm except that fumarate was not included. The conductivity of the fresh growth medium was 5.11 mS/cm.

Growing the Biofilms

Prior to inoculation, the three-electrode bioreactor was allowed to operate for 24 h to remove the initial oxygen from the system. The biofilm reactor was then inoculated with 20 mL of fumarate-free inoculum with the recycle and feed on. Within 24 h, the current began to increase and the biofilm was allowed to grow continuously. The biofilm was ready for microelectrode measurements at selected current values.

Polarizing the Biofilm Electrode

The biofilm electrode was polarized continuously using a potentiostat built in-house (Renslow et al., 2011). A selected potential of 0.45 $V_{Ag/AgCl}$ was used. Cyclic voltammograms were measured using a Gamry Reference 600™ potentiostat (Gamry Instruments, Warminster, PA).

Microelectrodes

Redox potential, pH, and graphite microelectrodes were used to characterize the microenvironments within *G. sulfurreducens* biofilms respiring on electrodes. The redox microelectrode (Fig. 3A), pH microelectrode (Fig. 3B), and measurement system have been described in detail previously (Babauta et al., 2011). Briefly, the redox and pH microelectrodes are potentiometric sensors. The redox microelectrode tip was made by electrochemically depositing platinum on a platinum microelectrode tip, resulting in a porous platinum ball with a large surface area. The redox microelectrode was calibrated using a standard YSI 3682 Zobell Solution (YSI Inc., Yellow Springs, OH). The pH microelectrode had a liquid ion-exchange membrane at the tip and was calibrated using standard buffer solutions (pH 4, 7, and 10) from ACROS Organic. The graphite microelectrode was similar to the redox microelectrode except that a single carbon fiber (catalog # C3005, World Precision Instruments, Inc., Sarasota, FL) was used to construct the microelectrode (Fig. 3C). The carbon fiber was covered with a thin layer of glass by pulling the glass and wire together. After pulling, the tip was ground to expose the graphite. The graphite microelectrode was placed in an outer casing, which allowed better imaging of the location of the microelectrode. A Ag/AgCl reference electrode was inserted into the outer case, which was also in contact with the growth medium. For redox, pH, and graphite microelectrode measurements, a Keithley 6517A electrometer/high resistance meter was operated as a high-resistance meter. The potential difference was read between the microelectrode tip and the reference electrode as indicated in Figure 3. The response time of each microelectrode was less than a few seconds.

Microelectrode Measurements

At selected current values, the three-electrode bioreactor was opened by removing the rubber stoppers above either the biofilm electrode or the counter electrode. To minimize oxygen intrusion into the system from the opened port, the headspace was continuously purged with the 80% N_2/20% CO_2 gas mixture. Once the microelectrode was positioned above the open port using micromanipulators, it was stepped down into the reactor volume just above the biofilm electrode or counter electrode. The microelectrode was then

positioned ~600 μm from the electrode surface and stepped down in 5-μm increments using custom microprofiler software. The locations of the microelectrode tip, the surface of the biofilm, and the electrode surface were located using a stereomicroscope (Zeiss Stemi 2000 stereomicroscope). It took several minutes to complete a profile in the biofilm. During the measurement of each profile, the measured current of the biofilm electrode was confirmed as being steady. During all microelectrode measurements, the biofilm electrode was polarized to 0.45 $V_{Ag/AgCl}$.

Acetate Determination

Acetate concentrations in the bulk medium of the three-electrode bioreactor were determined using high-performance liquid chromatography (HPLC). The system comprised a Hewlett Packard Series 1100 HPLC system (Agilent Technologies, Inc., Santa Clara, CA), outfitted with an automatic sampler (G1313A), a dual plunger quaternary pump (G131A), an online degasser (G1322A), and a diode array detector (G1315A). A hydrogen-form cation exchange column for small organic acids (Aminex HPX-87H, 300 mm × 7.8 mm) was used for separation. The column was maintained at 25°C, and the acetate was isocratically eluted with 5 mM H_2SO_4 (J.T. Baker ACS Reagent, 9681-03) prepared using HPLC-grade water (J.T. Baker, 4218-03) at a flow of 0.5 mL/min (Xie et al., 2011). Ultraviolet adsorption (260 nm) was used for peak detection, and ChemStation for LC 3D Systems software (Agilent Technologies, Inc.) was used for system control and data analysis. Acetate concentration was quantified by comparison to a linear calibration using the integrated peak areas of five analytical-grade acetate samples prepared in the fresh filter-sterilized growth medium described above.

The Local Biofilm Potential

The LBP was determined in a separate three-electrode bioreactor that allowed for microelectrode measurements longer than 1 day. A Gamry Series G™ 300 potentiostat (Gamry Instruments) was used to polarize the glassy carbon electrode (3 mm in diameter) when needed. The *G. sulfurreducens* biofilm was grown until a steady current was reached. The top of the three-electrode bioreactor was opened, and a graphite microelectrode (Fig. 3C) was manually placed inside the bulk solution using a micromanipulator. A flexible latex seal was then placed around the top of the bioreactor and the graphite microelectrode to maintain positive pressure inside the bioreactor. Using the micromanipulator, we moved the graphite microelectrode tip to a desired position inside the *G. sulfurreducens* biofilm. During this time, the OCP was monitored with a Keithley 6517A electrometer. After 2 days, the OCP reached a steady value; the graphite microelectrode was then connected to the working electrode and acted as a current collector inside the biofilm. The current was measured using the same electrometer in picoammeter configuration. When needed, cyclic voltammograms were measured using the Gamry Series G™ 300 potentiostat.

Results and Discussion

The microelectrode measurements were performed at least three different times at different locations in the biofilms. The results were all similar and led to identical conclusions. Here we show selected representative measurements.

Biofilm Growth, Current Generation, and Acetate Utilization

Figure 4A shows the variation of anodic current over time while the *G. sulfurreducens* biofilm grew. During the growth of the electrode-respiring *G. sulfurreducens* biofilm, we measured pH and redox potential inside the biofilm in two different growth phases, indicated by the red arrows in Figure 4A. The images inserted into Figure 4A show that the biofilm continued to grow after our first measurement and reached a thickness of

approximately 200 μm, which is significantly thicker than previously reported values (Franks et al., 2009; Jain et al., 2011; Liu et al., 2011). The current reached approximately 1.85 mA before our second measurement. An example of slow scan cyclic voltammetry (CV) (1 mV/s) of the *G. sulfurreducens* biofilm electrode is shown in Figure 4B. It is interesting to note that the steady state current measurements (15 min of constant current) were almost identical to the slow scan CV (reverse direction), as shown in Figure 4B. Above a polarization potential of 0.2 $V_{Ag/AgCl}$, a sustainable maximum current was generated by the *G. sulfurreducens* biofilm. Thus, the biofilm electrode was polarized to 0.45 $V_{Ag/AgCl}$ to ensure that we measured pH and redox potential in the region of limiting current and not where the current was dependent on the potential. These regions are represented as vertical dashed lines in Figure 4B. In addition to monitoring current, we also measured the bulk steady state acetate concentration and calculated the acetate utilization rate (Table I). The bulk steady state acetate concentration decreased from 20 to 17.6 mM at 1.05 mA and from 20 mM to 11.8 mM at 1.85 mA. Cumulatively, these data confirm that the *G. sulfurreducens* biofilm was actively consuming acetate and respiring on the electrode.

Profiles of pH at Two Different Currents on the Biofilm Electrode

The variation of pH by depth from the electrode is shown in Figure 5 for the two different biofilm growth phases corresponding to the different currents. As the current increased over time from 1.05 to 1.85 mA, the difference between the pH at the top of the biofilm and that at the bottom increased from 0.3 to 0.6 pH units. At the bottom of the biofilm, we observed minimum pH's of 6.5 and 6.3 for 1.05 and 1.85 mA, respectively. The variation in pH from the top of the biofilm to the bottom was consistent with the increased acetate utilization (Table I). A net increase in acetate consumption was predicted by Equation (3) to yield a net increase in protons and subsequently a decrease in pH

$$CH_3COO^- + 3H_2O \rightarrow CO_2 + HCO_3^- + 8H^+ + 8e^- \quad (3)$$

These pH profiles are in agreement with previous results in a *G. sulfurreducens* flow cell MFC (Franks et al., 2009). They observed a minimum pH of 6.2 at the bottom of a *G. sulfurreducens* biofilm during current flow. Our results, taken together with theirs, confirm the significant relationship between current generation and pH profiles in electrode-respiring biofilms in both MFCs and MECs.

We expected that the 200 μm thick biofilms should suffer from severe pH limitations. However, this was not the case. We observed a continually decreasing pH in the biofilm as current increased, suggesting that the current was not limited by pH at the time of the measurements. If the biofilm was always pH-limited, then the pH measured at the bottom of the biofilm would be the same regardless of the current. We make the distinction that not all biofilms are pH-limited and some undetermined parameter was controlling electron transfer when the biofilm was producing 1.05 mA of current. Recently, electron transfer in *G. sulfurreducens* biofilms was modeled using five electron transfer steps (Strycharz et al., 2011). The five electron transfer steps were: (1) mass transport of acetate, carbon dioxide, and protons; (2) microbial acetate consumption; (3) microbial reduction of a mediator; (4) extracellular electron transfer through the biofilm; and (5) oxidation of the mediator by the electrode. For any biofilm that is not pH-limited, any combination of these steps could limit current generation, although the authors suggest that step 4 is the most likely to be limiting. The conclusion that pH does not always control current generation lends itself to the prediction of current being limited by the biomass on the electrode (Picioreanu et al., 2010). While their model used thionine as an electron mediator, the results can be extended to the electrochemically active molecules utilized by *G. sulfurreducens* biofilms since the scan rate dependence under non-turnover conditions often shows a diffusion-like trend (Liu et al.,

2011; Strycharz et al., 2011). A weakness of both models that the authors state, however, is their inability to resolve the effect of pH inhibition on biofilm metabolism and therefore on current generation.

The growth rates of *G. sulfurreducens* cultures grown utilizing fumarate as an electron acceptor were observed to be reduced at pH 6.4 and 6, and completely inhibited at pH 5.5 (Kim and Lee, 2010). Thus, the bottom layer of the biofilm we studied could be considered pH-stressed such that growth is significantly reduced, although growth rates observed under non-electrode-respiring conditions extrapolated to electrode-respiring conditions may not be a realistic indicator of pH inhibition. Nonetheless, if a pH of <6 can be assumed to be complete pH inhibition as Torres et al. (2008b) postulated, then the *G. sulfurreducens* biofilm we studied did not experience complete inhibition, even at the bottom of the biofilm. This is corroborated by results obtained by Franks et al. (2009): when they changed the bulk pH from 6.9 to 6.15 they measured only a ~50% decrease in current (Fig. 7 in their article). The same trend was observed for a mixed culture biofilm dominated by *G. sulfurreducens* and showed further that current generation was completely inhibited at a bulk pH of 5 (Patil et al., 2010). One of the questions raised is “why does the pH seen in the *G. sulfurreducens* biofilms we studied never reach a pH of 5.5 or 5?” An individual layer of biofilm above the bottom layer would be expected to continue to generate protons regardless of the pH at the bottom layer, which would restrict buffer diffusion into the bottom layer, which would eventually reach complete pH inhibition (Torres et al., 2008b). One possible hindrance to this could be that the electron transfer mechanisms that provided a pathway for electrons from the top of the biofilm to the bottom layer have a pH dependence. For example, it was recently shown that the oxidation of PpcA, a well-studied periplasmic c-type cytochrome in *G. sulfurreducens*, facilitates proton transfer (Morgado et al., 2010). They calculated the pK_a of completely reduced PpcA and the pK_a of completely oxidized PpcA to be 8.6 and 6.5, respectively. From a thermodynamic point of view, a pH < 6.5 can inhibit proton transfer by PpcA, considering that protons transfer from regions of high proton concentration (low pH) to low proton concentration (high pH). Recent pH measurements inside the periplasm of *E. coli* showed that the periplasm pH was nearly the same as the external pH (Wilks and Slonczewski, 2007). Thus, it is possible that external pH can interfere with the function of PpcA in the periplasm of *G. sulfurreducens*, although measurements in *E. coli* may not be representative. A pH dependence was also shown in the conductivity of *G. sulfurreducens* biofilms (Malvankar et al., 2011). A second possibility is that increasing electron transfer resistance towards the top of the biofilm prevents the top layers from inhibiting the bottom layer (Jain et al., 2011). The interplay between proton transfer and electron transfer may not be simply controlled by buffer diffusion alone and warrants further investigation.

Proton flux can be estimated from the pH profiles by fitting our data with Fick's first law of diffusion (see SI—proton flux calculations). A value of $3.44 \times^{-4}$ nM $[H^+]$ s^{-1} cm^{-2} was calculated using the pH profile taken when the current was 1.85 mA. Proton flux can also be estimated independently using the measured current and Equation (3). For every eight moles of electrons generated, eight moles of protons are generated. Thus, 1.85 mA of current produces 3.07 nM $[H^+]$ s^{-1} cm^{-2}, a proton flux value 10,000 times greater than that estimated from the pH profile. The disparity in the estimated values can be explained by the equilibrium buffering effect described by Equation (4) (Fornero et al., 2010; Torres et al., 2008a)

$$H^+ + 8HCO_3^- \leftrightarrow 8CO_2 + 8H_2O \quad (4)$$

The protons generated by metabolism (Eq. 3) shift the equilibrium in Equation (4) to the right, consuming bicarbonate and diminishing the pH change inside the biofilm. Considering

that practically all proton transfer is due to buffer action, current values can be used to estimate the flux of either carbon dioxide or bicarbonate, or both, indirectly. However, Equation (3) predicts that for every eight moles of protons, one mole of carbon dioxide and bicarbonate is generated, which is approximately 0.38 nM $[CO_2]$ s^{-1} cm^{-2}. Because carbon dioxide, bicarbonate, and protons are also generated inside the biofilm under a pH gradient, it is difficult to analyze proton transfer mechanisms by interpreting current. Thus, direct measurements of carbon dioxide generation inside biofilms are necessary and may help to elucidate the proton transfer mechanisms in electrode-respiring biofilms as well as to close the carbon balance (Bester et al., 2010; Kroukamp and Wolfaardt, 2009).

Redox Potential Profiles at Two Different Currents at the Biofilm Electrode

Figure 5B shows two different redox potential profiles, measured at two different currents, 1.05 and 1.85 mA. The redox potential inside the biofilm increased from –500 to –460 $mV_{Ag/AgCl}$ and from –590 to –490$mV_{Ag/AgCl}$ at 1.05 and 1.85mA, respectively. This corresponds to redox potential increases of 30 mV at 1.05 mA and 100 mV at 1.85 mA. The inset in Figure 5B expands the data over a smaller *y*-axis range to show the redox potential change more clearly. When compared to the redox potential increase of 200 mV inside the biofilm predicted by Picioreanu et al. (2010), Figure 5B suggests that most of the current passing through the biofilm is not localized in the soluble aqueous phase and is unable to equilibrate with the redox microelectrode, consistent with the observation that replacing the growth medium does not affect current (Bond and Lovley, 2003). Otherwise, the redox potential profiles would have much larger changes for the given currents. A similar conclusion was drawn recently from spectroelectrochemistry in which the cytochrome heme redox centers in *G. sulfurreducens* biofilms were predominantly oxidized at positive polarization potentials (Jain et al., 2011; Liu et al., 2011). Our redox potential measurements may not directly show the oxidation states of cytochromes since (1) cytochromes have been shown to be associated with the biofilm matrix, (2) insufficient time was given for interaction between the biofilm and the microelectrode, and (3) the heme redox centers are typically inaccessible to equilibrium electrodes without the use of redox mediators (Dutton, 1978; Leang et al., 2010; Nevin et al., 2009). Instead, redox potential gives an indication of the overall redox state of the soluble environment around the cells and in the interstitial spaces of the biofilm.

That redox potential has been shown to correlate with electron acceptor availability in natural systems provides further insight into the measured redox potential profiles (McLatchey and Reddy, 1998). In natural systems, when electron donors or carbon sources are in excess, the electron acceptor available for specific types of metabolism typically controls redox potential by diffusion. Thus, a decreasing redox potential gradient towards the bottom of the biofilm is predicted by Equation (2) and is typically formed in stratified biofilms such as wastewater biofilms and microbial mats, since highly reduced electron acceptors must be shielded from oxidizing (more positive) redox potentials (Bishop and Yu, 1999; Tankere et al., 2002). For electrode-respiring biofilms, the redox potential would be expected to increase towards the source of the electron acceptor (biofilm electrode). Because the biofilm electrode was located at the bottom of the biofilm and acetate concentration in the bulk was in excess, the redox potential was expected to increase towards the bottom of the biofilm.

Profiles of pH and Redox Potential When Biofilm Is Removed

To further investigate the meaning of the pH and redox potentials inside the biofilm, we removed a small section of biofilm from the biofilm electrode and measured pH and redox potential profiles on the exposed electrode surface (Fig. 6 inset). Figure 6 shows that changes in pH and redox potential measured above the exposed electrode surface were

diminished to the point where they appeared negligible. The redox potential remained constant until the tip of the microelectrode touched the electrode surface. When the microelectrode was moved back to the inside of the biofilm, profiles similar to those in Figure 5 were measured. We conclude that the pH and redox potential profiles were associated only with the biofilm and not with the electrode itself. The pH and redox potential profiles in Figure 5 were caused by biofilm respiration and are not an artifact of current being drawn through the electrode as a whole.

Local Biofilm Potential

Redox potential measurements are a mixed potential measurement and are not selective towards any single redox couple present. However, when redox mediators are carrying high current densities in solution, we expect that they control the redox potential (Babauta et al., 2011). Since it was apparent that this was not the case, we used a different measuring concept, the LBP. We believed that there was a local potential associated with the biofilm matrix and that this LBP would more accurately describe the local redox state of the biofilm and biofilm matrix. Measuring the local redox state of the biofilm required that the microelectrode tip be electrically connected to the biofilm. We placed a graphite microelectrode tip inside the biofilm while it exchanged electrons with a larger glassy carbon electrode. After 2 days inside the biofilm (~100 μm away from the electrode surface), the OCP of the graphite microelectrode tip was consistently –185 $mV_{Ag/AgCl}$, which confirmed that the graphite microelectrode tip was not in contact with the larger glassy carbon electrode. Note that during that time, the tip of the microelectrode was not polarized and no current passed. We were unsure, however, whether the OCP value represented the LBP since the *G. sulfurreducens* biofilm had no advantage in electrically connecting with the unpolarized graphite microelectrode tip. We then polarized the graphite microelectrode tip to the same potential as the large glassy carbon electrode. The current was initially ~0 nA but increased to 26 nA within 3 days and to a maximum of 48 nA within 8 days (Supplementary Fig. SI-1). On the 3rd day, the CV shown in Figure 7 was obtained, and it was clear that electrons were transferring from the biofilm to the graphite microelectrode tip in a potential-dependent trend consistent with the large glassy carbon electrode and Figure 4B. When the graphite microelectrode was disconnected from the working electrode (no current passed), the OCP consistently read –405 $mV_{Ag/AgCl}$. This value corresponds to the OCP of graphite electrodes with *G. sulfurreducens* biofilms, which have been experimentally measured by us as ~–400 $mV_{Ag/AgCl}$, which is similar to typically reported values (Bond and Lovley, 2003). These results demonstrate that polarization of the microelectrode tip connected the tip to the biofilm matrix and allowed us to measure LBP. We believe LBP and the microelectrode we developed may play a critical role in measuring the conductivity of biofilm.

By placing a new sink for electrons inside the biofilm, we allowed the biofilm to connect electrically to the graphite microelectrode tip. Currently we do not know the mechanism of this electrical connection or how to quantify the nature of this connection in our system. However, considering previously published literature we speculate that it is due to the adsorption of c-type cytochromes or the establishment of nanowire-like structures connecting to the tip of the microelectrode (Malvankar et al., 2011). When the current was stopped and electrons accumulated in the biofilm, the LBP represented the biofilm potential where the biofilm was completely reduced (Jain et al., 2011; Liu et al., 2011). However, since the microelectrode worked inside the sphere of influence of a much larger electrode that was polarized, this assumption may not be true. The local biofilm previously transferring electrons to the graphite microelectrode tip within the biofilm may have used conduction to transfer electrons across a larger distance (Jain et al., 2011; Malvankar et al., 2011; Strycharz-Glaven et al., 2011). We expected to see a LBP more positive than –400

$mV_{Ag/AgCl}$ in the biofilm, considering the conductivity measurements of the biofilms. However, what we observed was counterintuitive. Even when current was passed, much of the biofilm was still in a reduced state; otherwise the LBP would have fallen between –400 mV and the polarization potential of the larger electrode. Perhaps these results demonstrate that the biofilm generated significant reducing current that could not be fully transferred to the large electrode surface and that, as a result, the LBP always reflected a potential near highly reducing conditions.

Measurements of pH and Redox Potential at Two Different Currents on the Counter Electrode

To characterize the whole three-electrode bioreactor and to help explain what we observed at the biofilm electrode, we also measured pH and redox potential at the counter electrode. Figure 8A shows two pH profiles measured at the counter electrode, at 1.05 and 1.85 mA. Near the surface the pH increased from the bulk value, from 7.3 to 7.4 at 1.05 mA and from 7.4 to 8.3 at 1.85 mA. This corresponds to pH increases of 0.1 and 0.9 at 1.05 mA and 1.85 mA, respectively. Unlike the biofilm electrode, there was convective transport due to the presence of hydrogen bubbles rising above the counter electrode (experimentally quantified). Thus, the pH profiles in Figure 8A are not diffusion-based profiles, which is reflected in the sharp change in slope at approximately 150 μm from the electrode. The increase in pH with increasing current generation indicates that protons were consumed faster than the buffer could react.

There was a larger pH change at the counter electrode than at the biofilm electrode, even with convective transport. A larger pH increase for the counter electrode would seem to point to the conclusion that if pH limitations exist in MECs, they first limit the counter electrode instead of the biofilm electrode. However, because our system was controlled by a potentiostat, any limitation of the counter electrode was negated by the potentiostat decreasing the polarization potential of the counter electrode. This does not affect our conclusions at the biofilm electrode. Instead, this highlights the relationship between counter electrode surface pH and potential. Table I shows this decrease in counter electrode potential, from –1.14 to –1.4 V as current increased from 1.05 to 1.85 mA. The same trend is seen in MECs that apply a constant potential using a DC voltage source (Geelhoed et al., 2010; Wang et al., 2010). For MECs with a constant applied potential, both the anode and the cathode potentials decrease during operation as current generation increases, which implies that there is an accumulation of electrons at the anode which the cathode cannot dissipate. Figure 8A explains this result as the cathode in these MECs being more limited by proton transport than the anode, making the cathode the limiting electrode and thereby increasing the cathodic energy loss (Lee and Rittmann, 2010ab). Thus in MECs used in practical applications, monitoring both the counter electrode potential and surface pH is important.

Figure 8B shows two different redox potential profiles at the counter electrode, at 1.05 and 1.85 mA. The redox potential at the counter electrode decreased from the bulk value, from –630 to –665 $mV_{Ag/AgCl}$ at 1.05 mA and from –680 to –770 $mV_{Ag/AgCl}$ at 1.85 mA. This corresponds to redox potential drops of 35 mV at 1.05 mA and 110 mV at 1.85 mA. In a three-electrode biofilm reactor, the counter electrode is an electron source and reduces any available electron acceptors. The most abundant electron acceptors in MECs are protons, and they are reduced to hydrogen as described by Equation (5)

$$2H^{+}+2e^{-} \rightarrow H_2, \qquad E^{0}= -615 \quad mV_{Ag/AgCl} \quad (5)$$

Hydrogen generation was confirmed above the counter electrode (Supplementary Fig. SI-2). The rate of hydrogen generation was high enough for it to be visually observed as bubbles coalescing on the counter electrode surface, which eventually rose to the liquid-headspace interface.

The pH profiles in Figure 8A show that the pH values very near the surface were higher than the bulk pH, indicating that the expected redox potential, according to Equation (2), is more negative. The proximity of the redox potential measurements to the standard reduction potential for protons in Equation (5) highlights an interesting fact about the cathodic reactions occurring at the counter electrode. In addition to the generation and circulation of hydrogen inside the three-electrode bioreactor, highly reduced solution is circulated. The presence of hydrogen at the anode has been shown to reduce the efficiency of MECs; however it is not clear what role the redox potential has in this effect (Torres et al., 2008a). There have been various literature studies using three-electrode bioreactors, often termed membraneless single-chamber reactors (Bouhenni et al., 2010; Fricke et al., 2008; Marsili et al., 2008; Strycharz et al., 2011). Many of these studies focused on the anode and controlled its potential but did not investigate the reactions at the counter electrode in detail. Considering our results, we believe studying electron transfer mechanisms in biofilm systems requires consideration of the reactions at the counter electrode. Introducing an ion-selective membrane into the bioreactor isolates the counter electrode at the cost of adding to the resistance to proton transfer. Our results indicate that more emphasis on the characterization of the type of bioreactor used should be applied in future electrode-respiring biofilm studies.

The pH and redox potential for the counter electrode and the biofilm electrode are plotted in Figure 9, where we observe distinct pH and redox potential microenvironments characteristic of interfacial phenomena. A microenvironment is defined as a microscale volume that has physical/chemical properties that are significantly different from those of the bulk solution. The presence of these microenvironments shows that biofilm reactors are more accurately characterized at the electrode surface. In Figure 9, we observe that the biofilm microenvironment tended to have a lower pH and less reducing conditions than the counter electrode microenvironment. The counter electrode operated near the theoretical stability limit for hydrogen evolution in an aqueous solution. This comparison is only approximate, however, since these measurements were made when current was passed. Surprisingly, the pH and redox potential data from inside the hole in the biofilm (Fig. 6) were aligned with the counter electrode despite being measured at the surface of the biofilm electrode when the biofilm produced 1.10 mA of current. This provides strong evidence that the bioreactor solution was dominated by the cathodic reaction occurring at the counter electrode.

Practical Implications

Compared to electron transfer, proton transfer inside electrode-respiring biofilms remains largely unknown because of the limited tools available for making direct measurements. While the concepts of proton transfer limitations and pH inhibition are not new and have been shown previously and the intimate coupling between electron transfer and proton transfer in biological redox systems is well documented, the effects of parameters such as current and biofilm thickness on the pH inside a biofilm have not been evaluated. Without knowing the distribution of pH inside a biofilm, characterizing the biofilm using voltammetry, in which redox proteins exhibit a pH dependence, may be difficult. Furthermore, the rate at which electrons move through a biofilm may be a function of pH and not simply of conductivity. Decoupling the effect of pH on electron transfer is a practical concern for studying electron transfer inside biofilms. Additionally, the role of soluble redox processes is less well-known. There is a significant amount of literature that

uses a three-electrode bioreactor configuration to study electron transfer mechanisms in biofilms (Harnisch et al., 2011; Jain et al., 2011; Liu et al., 2011; Peng et al., 2010; Strycharz et al., 2011; Torres et al., 2008b; Yi et al., 2009). Often the time it takes to grow the biofilms for these studies ranges from a few days to a few weeks and even up to a month (Bond and Lovley, 2003; Jain et al., 2011; Malvankar et al., 2011; Strycharz et al., 2011). In the present study, we found that soluble redox processes at the counter electrode dominated the redox potential. This could play a critical role in electron transfer mechanisms in long-term studies and in practical applications for natural systems.

Conclusions

In this work we quantified pH and redox potential variations in electrode-respiring *G. sulfurreducens* biofilms as a function of respiration rates, measured as current. In addition, we developed a new microelectrode to measure LBP. We conclude that for *G. sulfurreducens* biofilms grown under electrode-respiring conditions in a three-electrode bioreactor the redox potential increases from the top of the biofilm to the bottom. As in previous literature, the pH decreases from the top of the biofilm to the bottom. However, the pH continues to decrease in the biofilm through different growth phases, showing that the pH is not always a limiting factor in the biofilm. Additionally, the decreasing pH and increasing redox potential at the biofilm electrode are associated only with the biofilm, demonstrating that *G. sulfurreducens* biofilms respire in a unique internal environment. The LBP can be differentiated from the solution redox potential by placing a microelectrode inside the *G. sulfurreducens* biofilm acting as an electron sink. The LBP value corresponds to the OCP of graphite electrodes with attached *G. sulfurreducens* biofilms, which was experimentally measured by us to be around –400 $mV_{Ag/AgCl}$. Finally, limitations on pH are imposed at the counter electrode surface as current increases. For the first time, we measured pH variations at the counter electrode and demonstrated this directly.

Supplementary Material

Refer to Web version on PubMed Central for supplementary material.

Acknowledgments

This research is supported by the U.S. Office of Naval Research (ONR), grant #N00014-09-1-0090.

Contract grant sponsor: U.S. Office of Naval Research (ONR)

Contract grant number: N00014-09-1-0090

References

Babauta JT, Nguyen HD, Beyenal H. Redox and pH microenvironments within *Shewanella oneidensis* MR-1 biofilms reveal an electron transfer mechanism. Environ Sci Technol. 2011; 45(15):6654–6660. [PubMed: 21648431]

Bester E, Kroukamp O, Wolfaardt GM, Boonzaaier L, Liss SN. Metabolic differentiation in biofilms as indicated by carbon dioxide production rates. Appl Environ Microbiol. 2010; 76(4):1189–1197. [PubMed: 20023078]

Bishop PL, Yu T. A microelectrode study of redox potential change in biofilms. Water Sci Technol. 1999; 39(7):179–185.

Bond DR, Lovley DR. Electricity production by *Geobacter sulfurreducens* attached to electrodes. Appl Environ Microbiol. 2003; 69(3):1548–1555. [PubMed: 12620842]

Bond DR, Holmes DE, Tender LM, Lovley DR. Electrode-reducing microorganisms that harvest energy from marine sediments. Science. 2002; 295(5554):483–485. [PubMed: 11799240]

Bouhenni RA, Vora GJ, Biffinger JC, Shirodkar S, Brockman K, Ray R, Wu P, Johnson BJ, Biddle EM, Marshall MJ, Fitzgerald LA, Little BJ, Fredrickson JK, Beliaev AS, Ringeisen BR, Saffarini DA. The role of *Shewanella oneidensis* MR-1 outer surface structures in extra-cellular electron transfer. Electroanalysis. 2010; 22(7–8):856–864.

Coursolle D, Baron DB, Bond DR, Gralnick JA. The Mtr respiratory pathway is essential for reducing flavins and electrodes in *Shewanella oneidensis*. J Bacteriol. 2010; 192(2):467–474. [PubMed: 19897659]

Dutton, P. Redox potentiometry: Determination of midpoint potentials of oxidation–reduction components of biological electron-transfer systems.. In: Sidney, F.; Lester, P., editors. Methods in enzymology. Academic Press; New York, NY: 1978. p. 411-435.chapter 23

Fornero JJ, Rosenbaum M, Cotta MA, Angenent LT. Carbon dioxide addition to microbial fuel cell cathodes maintains sustainable catholyte pH and improves anolyte pH, alkalinity, and conductivity. Environ Sci Technol. 2010; 44(7):2728–2734. [PubMed: 20178380]

Franks AE, Nevin KP, Jia HF, Izallalen M, Woodard TL, Lovley DR. Novel strategy for three-dimensional real-time imaging of microbial fuel cell communities: Monitoring the inhibitory effects of proton accumulation within the anode biofilm. Energy Environ Sci. 2009; 2(1):113–119.

Fricke K, Harnisch F, Schroder U. On the use of cyclic voltammetry for the study of anodic electron transfer in microbial fuel cells. Energy Environ Sci. 2008; 1(1):144–147.

Geelhoed JS, Hamelers HVM, Stams AJM. Electricity-mediated biological hydrogen production. Curr Opin Microbiol. 2010; 13(3):307–315. [PubMed: 20206577]

Gorby YA, Yanina S, McLean JS, Rosso KM, Moyles D, Dohnalkova A, Beveridge TJ, Chang IS, Kim BH, Kim KS, Culley DE, Reed SB, Romine MF, Saffarini DA, Hill EA, Shi L, Elias DA, Kennedy DW, Pinchuk G, Watanabe K, Ishii S, Logan B, Nealson KH, Fredrickson JK. Electrically conductive bacterial nanowires produced by *Shewanella oneidensis* strain MR-1 and other microorganisms. Proc Natl Acad Sci USA. 2006; 103(30):11358–11363. [PubMed: 16849424]

Harnisch F, Koch C, Patil SA, Hubschmann T, Muller S, Schroder U. Revealing the electrochemically driven selection in natural community derived microbial biofilms using flow-cytometry. Energy Environ Sci. 2011; 4(4):1265–1267.

Jain A, Gazzola G, Panzera A, Zanoni M, Marsili E. Visible spectroelectrochemical characterization of *Geobacter sulfurreducens* biofilms on optically transparent indium tin oxide electrode. Electrochim Acta. 2011; 56(28):10776–10785.

Kim MS, Lee YJ. Optimization of culture conditions and electricity generation using *Geobacter sulfurreducens* in a dual-chambered microbial fuel-cell. Int J Hydrogen Energy. 2010; 35(23): 13028–13034.

Kroukamp O, Wolfaardt GM. CO(2) production as an indicator of biofilm metabolism. Appl Environ Microbiol. 2009; 75(13):4391–4397. [PubMed: 19346353]

Leang C, Qian XL, Mester T, Lovley DR. Alignment of the c-type cytochrome OmcS along pili of *Geobacter sulfurreducens*. Appl Environ Microbiol. 2010; 76(12):4080–4084. [PubMed: 20400557]

Lee HS, Rittmann BE. Characterization of energy losses in an upflow single-chamber microbial electrolysis cell. Int J Hydrogen Energy. 2010a; 35(3):920–927.

Lee HS, Rittmann BE. Significance of biological hydrogen oxidation in a continuous single-chamber microbial electrolysis cell. Environ Sci Technol. 2010b; 44(3):948–954. [PubMed: 20030379]

Liu H, Grot S, Logan BE. Electrochemically assisted microbial production of hydrogen from acetate. Environ Sci Technol. 2005; 39(11):4317–4320. [PubMed: 15984815]

Liu Y, Kim H, Franklin RR, Bond DR. Linking spectral and electro-chemical analysis to monitor c-type cytochrome redox status in living *Geobacter sulfurreducens* biofilms. Chemphyschem. 2011; 12(12):2235–2241. [PubMed: 21671335]

Logan BE, Hamelers B, Rozendal RA, Schrorder U, Keller J, Freguia S, Aelterman P, Verstraete W, Rabaey K. Microbial fuel cells: Methodology and technology. Environ Sci Technol. 2006; 40(17): 5181–5192. [PubMed: 16999087]

Malvankar NS, Vargas M, Nevin KP, Franks AE, Leang C, Kim BC, Inoue K, Mester T, Covalla SF, Johnson JP, Rotello VM, Tuominen MT, Lovley DR. Tunable metallic-like conductivity in microbial nanowire networks. Nat Nanotechnol. 2011; 6(9):573–579. [PubMed: 21822253]

Marsili E, Baron DB, Shikhare ID, Coursolle D, Gralnick JA, Bond DR. *Shewanella secretes* flavins that mediate extracellular electron transfer. Proc Natl Acad Sci USA. 2008; 105(10):3968–3973. [PubMed: 18316736]

McLatchey GP, Reddy KR. Regulation of organic matter decomposition and nutrient release in a wetland soil. J Environ Qual. 1998; 27(5):1268–1274.

Miller TL, Wolin MJ. A serum bottle modification of the hungate technique for cultivating obligate anaerobes. Appl Microbiol. 1974; 27(5):985–987. [PubMed: 4598231]

Morgado L, Bruix M, Pessanha M, Londer YY, Salgueiro CA. Thermodynamic characterization of a triheme cytochrome family from *Geobacter sulfurreducens* reveals mechanistic and functional diversity. Biophys J. 2010; 99(1):293–301. [PubMed: 20655858]

Nevin KP, Kim BC, Glaven RH, Johnson JP, Woodard TL, Methe BA, DiDonato RJ, Covalla SF, Franks AE, Liu A, et al. Anode biofilm transcriptomics reveals outer surface components essential for high density current production in *Geobacter sulfurreducens* fuel cells. PloS ONE. 2009; 4(5):>e5628. [PubMed: 19461962]

Patil SA, Harnisch F, Kapadnis B, Schroder U. Electroactive mixed culture biofilms in microbial bioelectrochemical systems: The role of temperature for biofilm formation and performance. Biosens Bioelectron. 2010; 26(2):803–808. [PubMed: 20630740]

Peng L, You SJ, Wang JY. Electrode potential regulates cytochrome accumulation on *Shewanella oneidensis* cell surface and the consequence to bioelectrocatalytic current generation. Biosens Bioelectron. 2010; 25(11):2530–2533. [PubMed: 20427175]

Picioreanu C, van Loosdrecht MCM, Curtis TP, Scott K. Model based evaluation of the effect of pH and electrode geometry on microbial fuel cell performance. Bioelectrochemistry. 2010; 78(1):8–24. [PubMed: 19523880]

Reguera G, Nevin KP, Nicoll JS, Covalla SF, Woodard TL, Lovley DR. Biofilm and nanowire production leads to increased current in *Geobacter sulfurreducens* fuel cells. Appl Environ Microbiol. 2006; 72(11):7345–7348. [PubMed: 16936064]

Renslow R, Donovan C, Shim M, Babauta J, Nannapaneni S, Schenk J, Beyenal H. Oxygen reduction kinetics on graphite cathodes in sediment microbial fuel cells. Phys Chem Chem Phys. 2011; 13(48):21573–21584. [PubMed: 22052235]

Rozendal RA, Hamelers HVM, Euverink GJW, Metz SJ, Buisman CJN. Principle and perspectives of hydrogen production through biocatalyzed electrolysis. Int J Hydrogen Energy. 2006; 31(12): 1632–1640.

Strycharz SM, Malanoski AP, Snider RM, Yi H, Lovley DR, Tender LM. Application of cyclic voltammetry to investigate enhanced catalytic current generation by biofilm-modified anodes of Geobacter sulfurreducens strain DL1 versus variant strain KN400. Energy Environ Sci. 2011; 4(3): 896–913.

Strycharz-Glaven SM, Snider RM, Guiseppi-Elie A, Tender LM. On the electrical conductivity of microbial nanowires and biofilms. Energy Environ Sci. 2011; 4(11):4366–4379.

Tankere SPC, Bourne DG, Muller FLL, Torsvik V. Microenvironments and microbial community structure in sediments. Environ Microbiol. 2002; 4(2):97–105. [PubMed: 11972619]

Torres CI, Lee HS, Rittmann BE. Carbonate species as OH(–) carriers for decreasing the pH gradient between cathode and anode in biological fuel cells. Environ Sci Technol. 2008a; 42(23):8773–8777. [PubMed: 19192796]

Torres CI, Marcus AK, Rittmann BE. Proton transport inside the biofilm limits electrical current generation by anode-respiring bacteria. Biotechnol Bioeng. 2008b; 100(5):872–881. [PubMed: 18551519]

von Canstein H, Ogawa J, Shimizu S, Lloyd JR. Secretion of flavins by *Shewanella* species and their role in extracellular electron transfer. Appl Environ Microbiol. 2008; 74(3):615–623. [PubMed: 18065612]

Wang AJ, Liu WZ, Ren NQ, Zhou JZ, Cheng SA. Key factors affecting microbial anode potential in a microbial electrolysis cell for H(2) production. Int J Hydrogen Energy. 2010; 35(24):13481–13487.

Wilks JC, Slonczewski JL. pH of the cytoplasm and periplasm of *Escherichia coli*: Rapid measurement by green fluorescent protein fluorimetry. J Bacteriol. 2007; 189(15):5601–5607. [PubMed: 17545292]

Xie R, Tu M, Wu Y, Adhikari S. Improvement in HPLC separation of acetic acid and levulinic acid in the profiling of biomass hydrolysate. Bioresour Technol. 2011; 102(7):4938–4942. [PubMed: 21316945]

Yi HN, Nevin KP, Kim BC, Franks AE, Klimes A, Tender LM, Lovley DR. Selection of a variant of *Geobacter sulfurreducens* with enhanced capacity for current production in microbial fuel cells. Biosens Bioelectron. 2009; 24(12):3498–3503. [PubMed: 19487117]

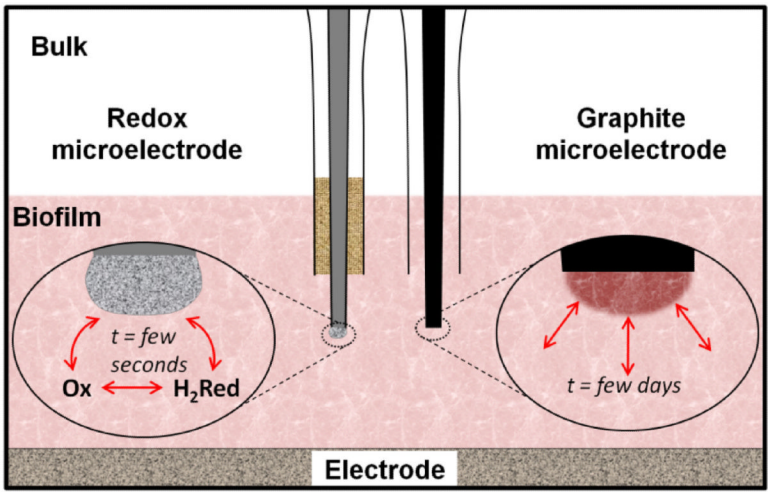

Figure 1.

Diagram of redox and biofilm potentials. A biofilm is grown on top of the electrode. The potential of this electrode against a reference electrode is called the biofilm electrode potential. A microelectrode with a Pt tip is inserted into the biofilm. The Pt tip equilibrates with the redox-active compounds within the biofilm, and the potential under this condition is called the redox potential. A microelectrode with a carbon fiber tip is inserted into the biofilm, and after the carbon fiber tip is polarized, the tip connects electronically to the biofilm. The potential under no-current conditions after the biofilm is electronically connected to the microelectrode tip is called the local biofilm potential (LBP).

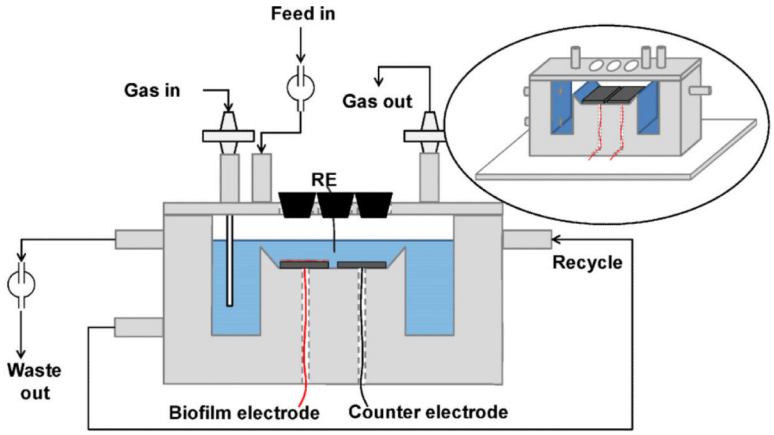

Figure 2.
A three-electrode bioreactor. The working, counter, and reference electrodes were housed in the same compartment. The inset shows a perspective view.

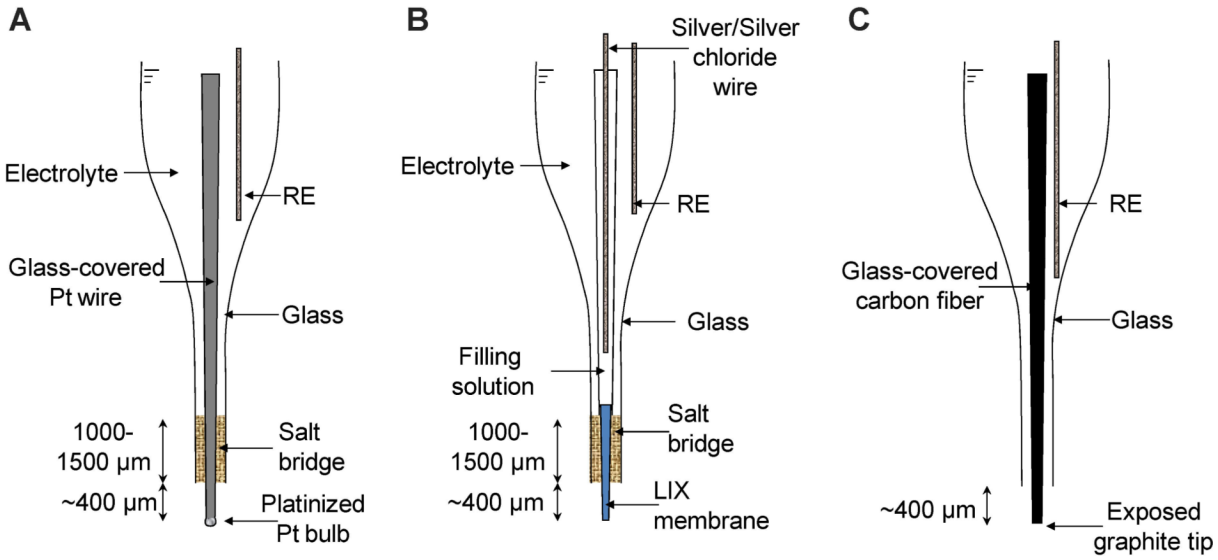

Figure 3.

A: Redox microelectrode, (**B**) pH microelectrode, and (**C**) graphite microelectrode. RE represents the Ag/AgCl reference electrode.

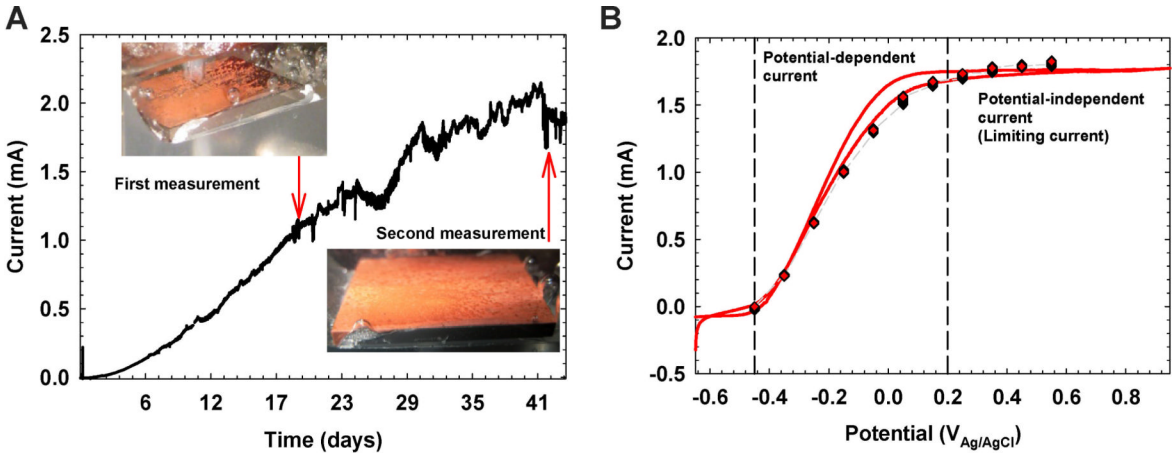

Figure 4.

A: Current generation of the *G. sulfurreducens* biofilm over time. The red arrows show the times when the pH and redox potential profiles were measured inside the biofilm. The images show the biofilm during measurement. **B**: Steady state polarization curve superimposed on slow-scan CV (1 mV/s). At polarization potentials above 0.2 $V_{Ag/AgCl}$, a maximum current is achieved.

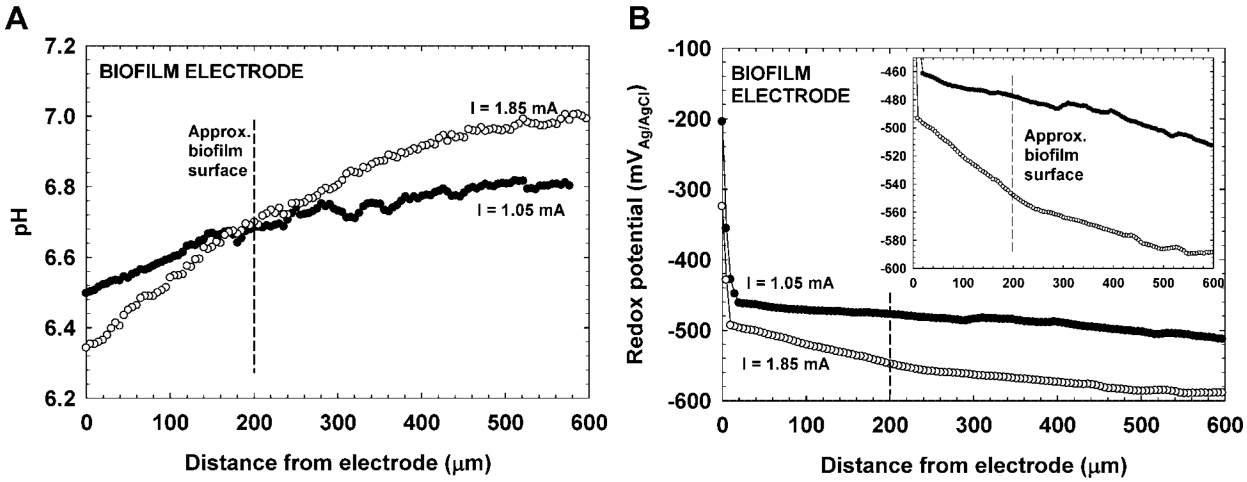

Figure 5.

A: The pH profiles at the biofilm electrode. **B**: The redox potential profiles at the biofilm electrode. The inset shows the profiles over a smaller *y*-axis range for clarity. The biofilm electrode was polarized to 0.45 $V_{Ag/AgCl}$ during measurements. The filled in-circles represent profiles measured at 1.05 mA. The open circles represent profiles measured at a current density of 1.85 mA.

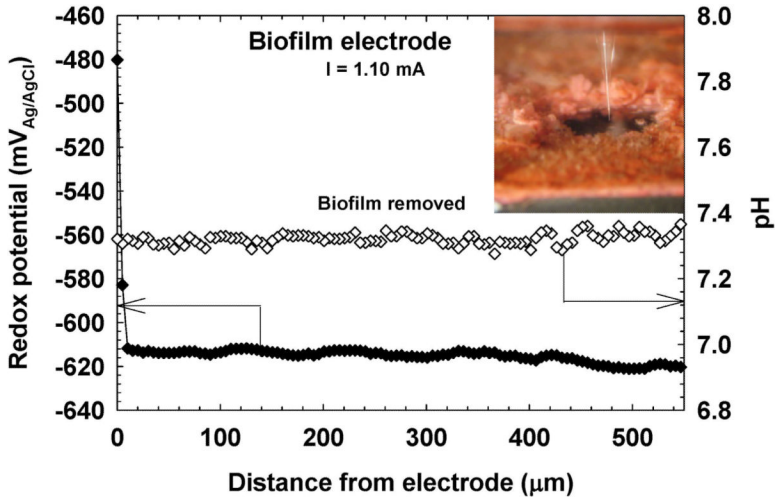

Figure 6.

Measurements of pH and redox potential above an exposed biofilm electrode surface. The inset shows a microelectrode measuring a profile above the exposed electrode surface. The redox potential remained constant until it touched the electrode surface.

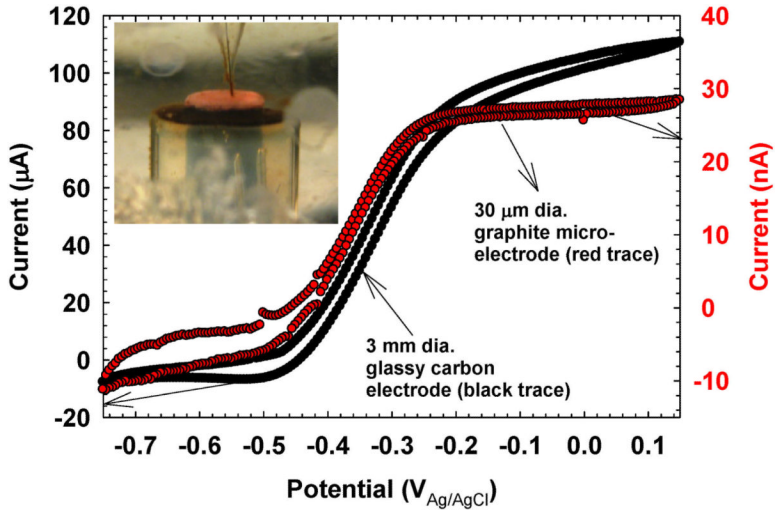

Figure 7.

CV of a *G. sulfurreducens* biofilm at a large glassy carbon electrode (black trace) and at a graphite microelectrode tip inserted into the same biofilm (red trace). The inset shows the graphite microelectrode tip inserted into the *G. sulfurreducens* biofilm.

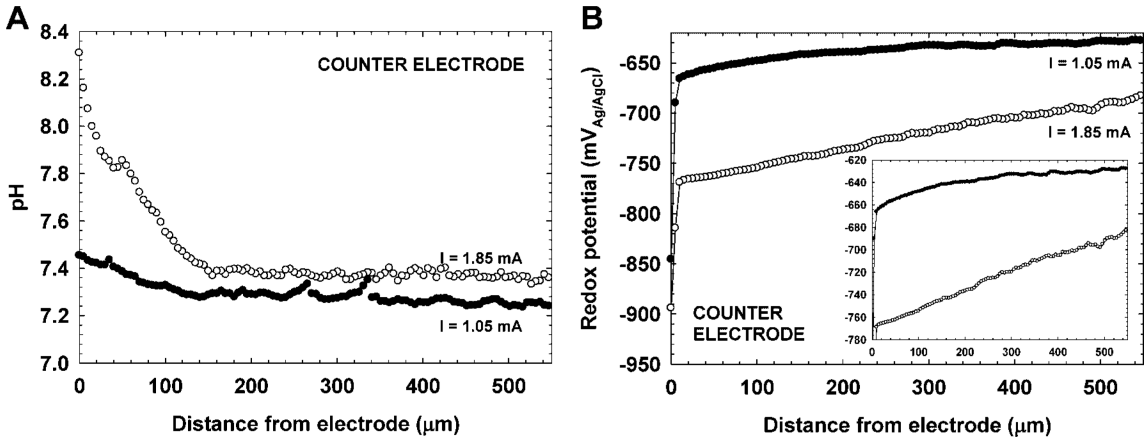

Figure 8.

A: pH profiles at the counter electrode. **B**: Redox potential profiles at the counter electrode. The inset shows the profiles over a smaller *y*-axis range for clarity. The biofilm electrode was polarized at +450 $mV_{Ag/AgCl}$ during measurements. The filled-in circles represent profiles measured at 1.05 mA, and the open circles represent profiles measured at a current density of 1.85 mA.

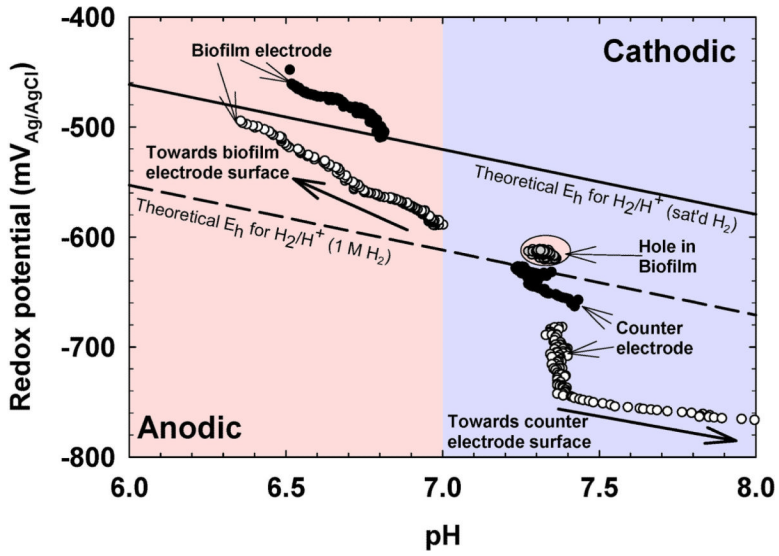

Figure 9.

Comparison of all pH and redox potential profiles with the theoretical redox potential and pH relationship for the H_2/H^+ redox couple using Equation (2). Redox potential is abbreviated as E_h for clarity.

Table I

Biofilm and counter electrode potentials and acetate concentrations.

	***I* = 1.05 mA**	***I* = 1.85 mA**
Biofilm electrode potential	0.45 $V_{Ag/AgCl}$	0.45 $V_{Ag/AgCl}$
Counter electrode potential	–1.14 $V_{Ag/AgCl}$	–1.4 $V_{Ag/AgCl}$
Feed acetate concentration	20 mM	20mM
Bulk steady state acetate concentration	17.6 mM	11.8 mM
Acetate utilization rate	1.46 mmol/h	5.00mmol/h